Construction and Building Materials 134 (2017) 610–616

Contents lists available at ScienceDirect

Construction and Building Materials

journal homepage: www.elsevier.com/locate/conbuildmat

Low-pressure silica injection for porosity reduction in cementitious materials

Riccardo Maddalena, Andrea Hamilton *

Department of Civil and Environmental Engineering, University of Strathclyde, Glasgow, United Kingdom

HIGHLIGHTS

- A novel non-destructive technique for cement surface treatment has been developed and proven effective under laboratory conditions.
- Nano-silica and silica fume can successfully penetrate the cement surface within 14 days and create extra C-S-H.
- Silica injections are carried out at low-pressure, ca. 20 kPa and this is the first demonstration of a simply applied and effective technique.

GRAPHICAL ABSTRACT

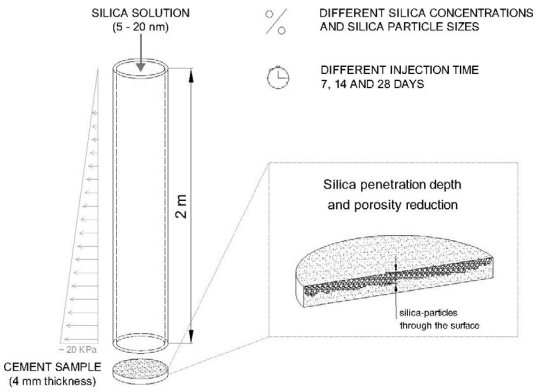

ARTICLE INFO

Article history:
Received 5 August 2016
Received in revised form 20 October 2016
Accepted 3 November 2016
Available online 06 January 2017

2010 MSC:
00-01
99-00

Keywords:
Porosity
C-S-H
Portlandite

ABSTRACT

The durability of building materials is related to the presence of cracks as they provide a fast pathway for the transport of liquid and gases through the structure. Restoration and preservation of historic buildings are the potential applications of this novel technique which uses nano-silica and silica fume particles for consolidation. The small particle size range and the high reactivity of nanoparticles allow them to interact with calcium sources naturally present in cement and concrete, forming binding and strengthening compounds such as calcium silicate hydrate. Nanoparticles act as a crack-filling agent, reducing the porosity and increasing the durability of existing materials. In this study we describe the injection of nano-silica, under low water pressure, into hydrated cement paste. This novel technique can tailor the mechanical and hydraulic properties of existing building materials using a simple and non-destructive procedure.

1. Introduction

Most of the built environment uses cement or concrete in some way, and many iconic buildings constructed in 1920s and later suffer from crack formation, water penetration and damage mechanisms such as alkali-silica reaction. Cracking in concrete and mortar is an inevitable phenomenon of ageing and erosion. Thus, material characteristics such as porosity, permeability and strength are altered during ageing. Hardened concrete and cement contain two important mineral phases: calcium hydroxide (portlandite) and calcium silicate hydrate (C-S-H), the former has a defined crystalline structure, the latter is semi-crystalline [14]. C-S-H is the phase responsible for strength development in concrete

* Corresponding author.
E-mail address: andrea.hamilton@strath.ac.uk (A. Hamilton).

http://dx.doi.org/10.1016/j.conbuildmat.2016.11.016
0950-0618/

and can form up to 70% of the total volume of hardened concrete [4]. C-S-H is produced by hydration of alite and belite (impure tricalcium silicate and dicalcium silicate respectively) which are present in cement clinker. Pozzolanic materials such as fly ash, rice husk ash and silica fume can also be added, resulting in the production of more C-S-H and improved mechanical performance [18,16]. The formation of cracks and increased porosity from leaching in concrete and cement paste presents an easy pathway for the ingress of moisture. Gaps and cracks can be reduced by application of nanoparticle consolidants. In the work presented here, the injected silica reacts with portlandite naturally present in hydrated cement paste to form new C-S-H and reduce the porosity of the system. The result is decreased permeability and potentially increased durability of the cement [3,8,17,9]. Research on partial replacement of cement clinker with nano-silica [13] found that increasing the quantity of nano-silica replacing cement from 3 vol.% to 5 vol.%, produced a mortar with higher mechanical strength by acceleration of the hydration reaction and the filler effect of nano-particles. In addition, the hydrated paste had a dense and compact texture and an absence of portlandite crystals was observed, suggesting that most of the calcium hydroxide reacted with the nano-silica added [13,10,15]. Nano-silica addition to cement paste increases C-S-H formation and accelerates hydration of unreacted alite (C_3S), due to the high reactivity of small particles [2]. An average water penetration depth of 14.6 cm in concrete made with fly ash and cement under low applied pressure was observed, whereas a water penetration depth of 8.1 cm in the same concrete mixed with nano-silica under high applied pressure was recorded, confirming the improvement in water penetration resistance with nano-silica addition [10]. It was concluded that the pozzolanic reaction of fly ash in the presence of nano-silica produces C-S-H faster and earlier compared to ordinary Portland cement (OPC) mixed with fly ash but no nano-silica. Varying the nano-silica content (3 wt.%, 6 wt.%, 10 wt.%, and 12 wt.%) in mortar produces an increase in strength correlated with a decrease in calcium hydroxide content. The heat of hydration is also increased by addition of nano-silica due to the rapid hydration of silicates [11]. Nano-silica surface treatments have been investigated using electro-kinetic deposition, nanoparticle coating, brushing, etc. A reduction in permeability was observed by Cardenas et al., for low alkali cement paste with 0.8 w/c ratio and impregnated with colloidal alumina by electro-phoresis [3]. Pore size refinement by reduction in the pore volume of treated samples with higher w/c ratio was also observed. The effect of curing temperature on hardened cement paste treated with nano-silica and tetraethoxysilane (TEOS) under sealed and unsealed conditions was studied [8]. Hou et al. found that mortar samples cured at 50 °C and treated with nanosilica/TEOS show a reduction in water absorption compared to samples treated in the same way but cured at 20 °C. High temperature curing contributes to the production of additional C-S-H gel and reduction of calcium hydroxide, which results in smaller capillary pores and finer gel pores. The transport properties of cement pastes with varying w/c ratio and surface treated with nano-silica and TEOS were also investigated. The water absorption and water vapour permeability are decreased by incorporation of nano-silica and TEOS in mortar with higher w/c ratio. Hardened mortar, surface treated by nano-silica using electro-migration, showed reduced cumulative porosity, and a higher rate of pozzolanic reaction was confirmed by the reduction in portlandite content [17]. While the application of nano-particles to cement and concrete surfaces has been shown to have beneficial effects on cement durability, very little research has been conducted on developing low cost and non-destructive techniques for concrete surface treatment. The aim of this work was to investigate a non-destructive and easily applied conservation treatment for cracked or friable concrete which is relevant to infrastructure conservation, ranging from buildings to bridges and more specialist applications in nuclear waste containment ponds. In this study the effect of nano-silica and silica fume injection in hardened cement paste was investigated by quantitative analysis of the resulting hydration products (C-S-H and portlandite) present.

2. Materials and methods

2.1. Materials

All experiments were carried out on pure hardened cement paste, made using ordinary Portland cement CEM II/A-L, class 42.5 N (physicochemical properties are listed in Table 1) and deionized water. Samples were treated with nano-silica (NS) suspension, LUDOX T-50, or silica fume (SF), ELKEM microsilica. Their chemical properties are detailed in Table 2.

2.2. Sample preparation

Cement samples were prepared by mixing Portland cement and deionized water at a water to cement (w/c) ratio of 0.41. Cement paste was mixed in a rotary mixer according to BS EN 196-1:2005 before being cast into plastic moulds (35 mm ø and 4 mm thickness) and cured under controlled conditions (relative humidity of 98 ± 2% and temperature of 21 ± 2 °C). After 28 days, cement discs were oven-dried at 60 °C for ca. 100 h, or until mass change was negligible. The aim of this experiment was to measure silica entrainment through the pore structure, rather than conduct accurate micro-structural analyses. Therefore, relatively gentle, oven drying at 60 °C was considered adequate for a comparative study of silica imbibition.

2.3. Experimental design

Nano-silica injection was carried out by varying three parameters: injection period, concentration of silica suspension injected, and silica particle size (NS or SF), using a constant applied pressure head. Silica solutions were prepared using nano-silica stock suspension or solid silica fume, mixed with deionized water. In order to investigate how the penetration depth in the disc varies with nano-silica content, three different suspension concentrations (10 wt.%, 15 wt.% and 20 wt.%) were used, for a total injection time of 14 days. The effect of injection time was determined by keeping cement discs under constant hydrostatic injection for 7, 14 and 28 days using 10 wt.% nano-silica colloidal suspension. To compare the reactivity and effect of particle size on penetration depth, samples were injected with 10 wt.% and 20 wt.% suspensions of silica fume or nano-silica for a period of 14 days (Table 3). The cement

Table 1
Characteristic of CEM II/A-L (Class 42.5 N) Portland cement (according to the certificate of conformity, test method BS EN 196-2).

Components	CEM II (%)
Clinker	80–94
Gypsum added	4.0
Limestone	6–20
Chemical composition (>0.2%)	
SiO_2	18.2
Al_2O_3	4.5
Fe_2O_3	2.6
CaO	64.0
MgO	1.3
SO_3	2.3
Na_2O	0.23
Solid density (kg/m^3)	3100
Specific area (m^2/g)	0.41
Compressive strength at 28 day (MPa)	57.5

Table 2
Characteristics of nano-silica (NS) and silica fume (SF) as purchased from suppliers.

Components	NS	SF
State	Aqueous suspension	Densified
Chemical composition (>0.2%)		
SiO_2	50 wt.%	99.9 wt.%
Water	50 wt.%	–
Particle size diameter (nm)	5–20	150–1000
Density (g/cm^3)	1.4	1.56
Specific surface area (m^2/g)	160	21.5

disc was fixed in place at the bottom of a PVC pipe of 2 m length and 40 mm internal diameter (Fig. 1), the pipe was then clamped vertically in a retort stand. The solution of nano-silica at a given concentration was slowly poured into the pipe from the top, to minimise the density gradient. The length of pipe used gives a constant hydrostatic pressure of 20 kPa at the bottom of the pipe, where the OPC specimen is placed. After filling the pipe, a plastic cap was placed at the top of the pipe to avoid evaporation of the suspension. At the end of the injection period the disc was removed and oven-dried at 60 °C for ca. 100 h, or until mass change was negligible. The sample weight was recorded before and after the injection to determine the mass of silica added to the pores.

2.4. Characterisation

The efficacy of injected silica to react with calcium hydroxide (CH) present in the hydrated cement paste to form additional calcium silicate hydrate (C-S-H) was determined by the quantity of calcium hydroxide and calcium silicate hydrate in the treated hydrated cement paste compared with the control sample. An average of 20 mg was sampled from the cross section of the disc and powdered for thermogravimetric analysis. Thermal analyses were conducted at a heating rate of 10 °C min^{-1} from 25 °C to 1000 °C under nitrogen gas flow, using a Netzsch simultaneous analyser. Mineralogical composition of silica injected specimens was analysed by powder X-ray diffraction (XRD) using a Bruker D8 Advance diffractometer, from 5° to 60° 2θ, at a rate of 1° min^{-1} and a step size of 0.02° 2θ. To determine silica entrainment through the pores, sample disc mass was recorded before and after silica injection, on samples oven dried at 60 °C. Open porosity (φ) was determined by measuring the total water content in each sample (in three replicates) after oven-drying at 60 °C followed by overnight saturation in a vacuum chamber. Open porosity was calculated using Eq. (1):

$$\varphi = \frac{m_s - m_d}{V \cdot \varrho} \quad (1)$$

where φ is the open porosity, m_s is the saturated sample mass (kg), m_d is the oven dried mass (kg), V is the volume of the sample (m^3) and ϱ is the density of water at 20 °C (kg m^{-3}). The open porosity value is the average of three measurements of the complete sample

Table 3
Experimental parameters and sample details.

Sample	Injected silica NS or SF	Silica content (wt.%) in suspension	Injection period, days
S10-7	NS	10	7
S10-14	NS	10	14
S15-14	NS	15	14
S20-14	NS	20	14
S10-28	NS	10	28
SF10-14	SF	10	14
SF20-14	SF	20	14

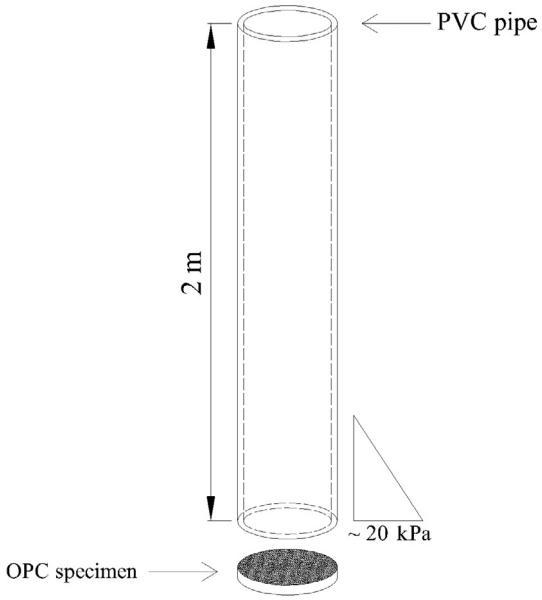

Fig. 1. Schematic diagram of experimental set-up.

disc, broken into three pieces for testing. Sample microstructure was imaged using Scanning Electron Microscopy (FEG-SEM, Hitachi SU6600) and Energy Dispersive Spectroscopy (EDS, Oxford INCA-7260) with an accelerating voltage of 10–15 keV. All samples were resin impregnated, polished and gold coated. The penetration depth of the silica after injection was also estimated by SEM imaging (Fig. 2).

3. Results

3.1. Mass change and porosity measurements

Mass measurements showed that after 14 days of nano-silica injection, the mass increase is directly proportional to the concentration of the silica suspension used (Fig. 3). At a given nano-silica content in the pipe of 10 wt.%, the sample mass shows an exponential trend reaching 2.0 wt.% mass gain after 28 days (Fig. 3). A comparison between nano-silica and silica fume show the effect of particle size on the injection: doubling the concentration of nano-silica results in a mass increase of ca. +1% of the original value, whereas doubling the silica fume content results in an increase of ca. +0.1%. This is probably due to the low particle size range of nano-silica (5–20 nm), able to penetrate into smaller pores. Open porosity (φ) measurements show that an increase in nano-silica content in the solution produces a significant decrease in porosity of ca. 30%, from the initial value (sample OPC, $\varphi = 0.30$) to the highest concentration at 20 wt.%. (sample S20-14, $\varphi = 0.21$), as shown in Fig. 4. Injection of silica-fume, does not produce a significant porosity reduction [15]. Injection time at the lowest nano-

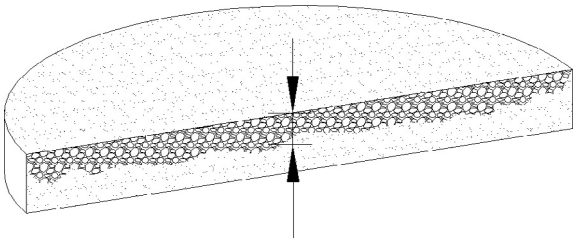

Fig. 2. Model of silica penetration depth on OPC sample after injection.

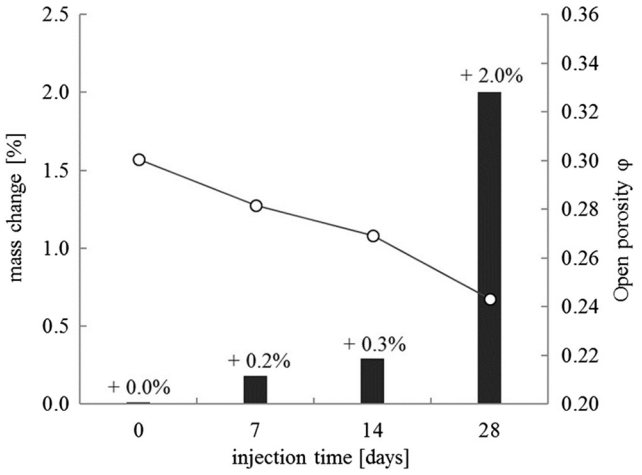

Fig. 3. Influence of injection time on mass increase and open porosity using a 10 wt. % nano-silica suspension. Bars represent mass change and open circles represent porosity values.

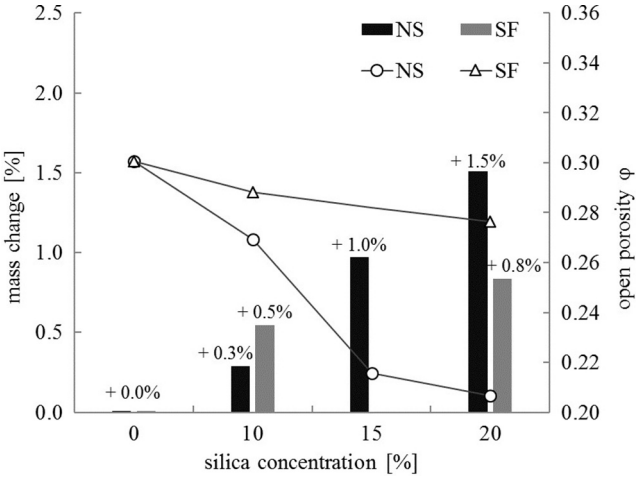

Fig. 4. Influence of silica suspension concentration on mass increase and open porosity after injection for 14 days. Bars represent change. Open circles and triangles represent porosity values.

silica suspension concentration (10 wt.%) shows a reduction in porosity of ca. 20%, from the initial value (sample OPC, $\varphi = 0.30$) to the longest injection time (sample S10-28, $\varphi = 0.24$) as shown in Fig. 4.

3.2. Thermogravimetric analysis and XRD analysis

Fig. 5 shows the thermogravimetric (TG) curves for selected samples. The mass loss is in wt.% with respect to temperature (25–1000 °C). All samples show TG curves typical of Portland cement, displaying maximum mass loss from room temperature to 200 °C. The mass loss in the range 80–150 °C is attributed to C-S-H gel, calcium aluminate silicate hydrate (C-A-S-H) gel, ettringite and other minor compounds [19,20,12]. The thermogravimetric step in the range 400–460 °C is assigned to portlandite dehydration (CH). Mass loss over the range 530–660 °C may be attributed to the loss of CO_2 from any calcium carbonate present. All samples show a slight mass loss in the range 700–780 °C due to the dehydroxylation of silanol Si-O-H groups [20,6]. Table 4 gives the TG values in the C-S-H and portlandite range calculated using Eq. (2):

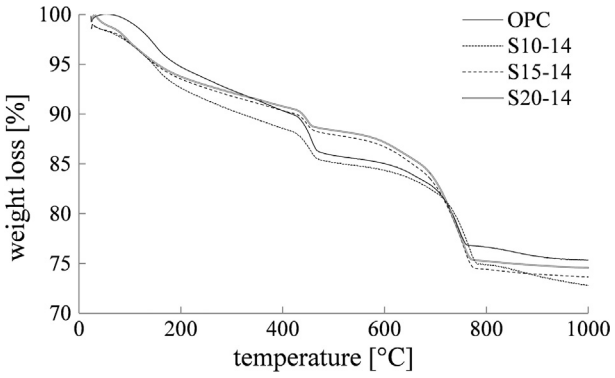

Fig. 5. Thermogravimetric curves of OPC control and S10-14, S15-14 and S20-14 samples.

Table 4
Summary of the TG results for each sample. S represents nano-silica and SF represents silica fume.

Sample	C-S-H 80–150 °C (% mass loss)	CH 400–460 °C (% mass loss)	Water 30–550 °C (% mass loss)
OPC	2.89	3.35	14.21
S10-7	2.80	2.70	13.68
S10-14	3.02	2.68	14.09
S15-14	3.04	1.96	11.34
S20-14	3.09	2.03	11.99
S10-28	2.81	2.15	12.09
SF10-14	2.80	2.25	12.72
SF20-14	3.01	2.09	12.61

$$m = m_{T_i} - m_{T_f} \quad (2)$$

where m is the mass loss in wt.% in the defined temperature range ($T_i - T_f$), m_{T_i} is the mass loss at the initial temperature T_i and m_{T_f} is the mass loss at the final temperature T_f. Water mass loss up to 550 °C is given to represent the loss of all pore and chemically bound water.

Fig. 9 shows the reduction of portlandite as it reacts with nano-silica to form additional C-S-H, which can be quantified by XRD analysis. This reduction of portlandite by ca. 40% from the initial portlandite content is higher in comparison with the values found in literature [3,17], due to a longer treatment time and higher applied pressure. There is no evidence of increased portlandite reduction when the nano-silica suspension concentration is increased beyond 15 wt.% in the injecting solution. The total increase of C-S-H formed, ca. 20% with respect to the original value, is over-estimated, due to the presence of other minor compounds in the same temperature range (80–150 °C). Accurate estimation is given by semi-quantitative analyses of XRD patterns. Fig. 10 suggests that the ideal injection period is 14 days, producing a portlandite reduction of ca. 40%. TG analysis of nano-silica and silica fume for 14 days injection time show that both materials offer a comparable CH reduction at the highest concentration (20 wt.%).

XRD analysis of the injected samples (Fig. 6) show a progressive decrease in intensity of portlandite and calcium aluminate phase reflections. Calcium aluminate phases (C_3A, peak at ca. 11.5° 2θ), present in the original clinker reacted with nano-silica forming additional C-S-H or C-A-S-H (calcium aluminate silicate hydrate), observed at ca. 15.5° 2θ. As shown in Figs. 7 and 8, the XRD patterns are plotted as intensity difference compared to the OPC control sample. The more negative the intensity of the peak, the lower the phase content is. One can see the effect of silica concentration on the intensity of reflections. Decrease in the intensity of the main reflection of portlandite (peak at ca. 18° 2θ) and increase in C-S-H

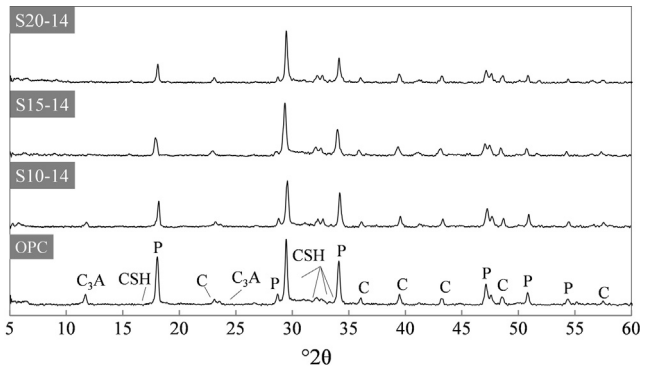

Fig. 6. XRD analysis of selected samples. List of the major mineral phases. [P: portlandite; C: calcite; C_3A: calcium aluminate; CSH: calcium silicate hydrate].

reflections (ca. 29.4–32.5° 2θ) are shown in Fig. 8. Semi-quantitative analyses of XRD patterns were carried out by integrating the area of the peaks corresponding to each mineral phase. Results are shown in Figs. 9 and 10. A CH reduction of ca. 40% from the blank sample using the highest silica concentration (20 wt.% solution) has been calculated, confirming the value obtained by thermogravimetric analysis. A relative increase of 15% C-S-H was formed after 14 days in accordance with the TGA values.

3.3. SEM analysis and water transport

Backscattered electron images give qualitative information on silica penetration depth and show densification of the matrix. It was measured along the direction of silica injection (horizontally left to right in the BSE images). With increasing nano-silica content an increase of penetration depth was observed: ca. 500 μm, 630 μm and 740 μm respectively for samples S10-14, S15-14 and S20-14, as shown in Fig. 11 To understand particle penetration depth we calculated flow through the blank specimen and linear particle diffusion. Using Darcy's law (Eq. (3)), flow through the blank specimen was calculated in $m^3\ s^{-1}$.

$$Q = k_s \frac{\Delta h}{L} A \tag{3}$$

where k_s is the saturated permeability ($m\ s^{-1}$), L is the thickness of the specimen (in mm), A is the cross sectional area of the sample ($38.48\ mm^2$) and Δh is the hydraulic head (2000 mm). The value of k_s ($1 \cdot 10^{-13}\ m\ s^{-1}$) was taken from Christensen et al. [5] for hardened cement paste aged 28 days with w/c ratio of 0.47. The volumetric flow through the sample is $0.416\ mm^3\ day^{-1}$. After 14 days the calculated total volume of water in the blank specimen is $0.0058\ cm^3$, which is considerably less than the pore volume of the sample, $1.1545\ cm^3$ and explains why water does not penetrate through the blank specimen after 14 days. The flow velocity in $cm\ day^{-1}$ is $4.32 \cdot 10^{-4}$ indicating that the penetration depth of water into a blank specimen would be 0.06 mm (60 μm) after 14 days. Particle diffusivity was calculated using the Stokes-Einstein equation (Eq. 4):

$$D = \frac{k_B T}{6\pi\eta r} \tag{4}$$

where D is the diffusivity of a particle in a straight line ($m^2\ s^{-1}$), k_B is Boltzmann's constant, T is the temperature in kelvin, r is the radius of the smallest particle size (5 nm diameter) and η is the viscosity of the carrier medium, which is water in this case (Pa s). Calculated particle diffusivity is $9.82 \cdot 10^{-11}\ m^2\ s^{-1}$. Using Eq. (5), it is possible to calculate the distance traveled, x, as function of the diffusivity D and time t.

$$x = \sqrt{D \cdot t} \tag{5}$$

The distance travelled after 14 days by the smallest particle is 344 μm. This value does not take into account the tortuosity (ξ) of the structure. If we assume $\xi = 3$ [7], then the distance travelled by the smallest particle is 115 μm which fits reasonably well with the penetration depth of 500–740 μm estimated using SEM images. From mass measurements after particle infiltration and after careful drying of the specimen, the lowest calculated porosity reached, for any sample, is $\varphi = 0.284$. From TGA analysis and semi-quantitative XRD results we calculate the volume of C-S-H gel produced (using a C-S-H density value of 2.6 from Allen et al. [1]) and the calculated open porosity of sample S20-14 reduces to $\varphi = 0.25$ by pore closing. The measured porosity of the blank specimen and sample S20-14 are 30% and 21% respectively. We suggest the lower measured porosity, compared with the calculated porosity, may

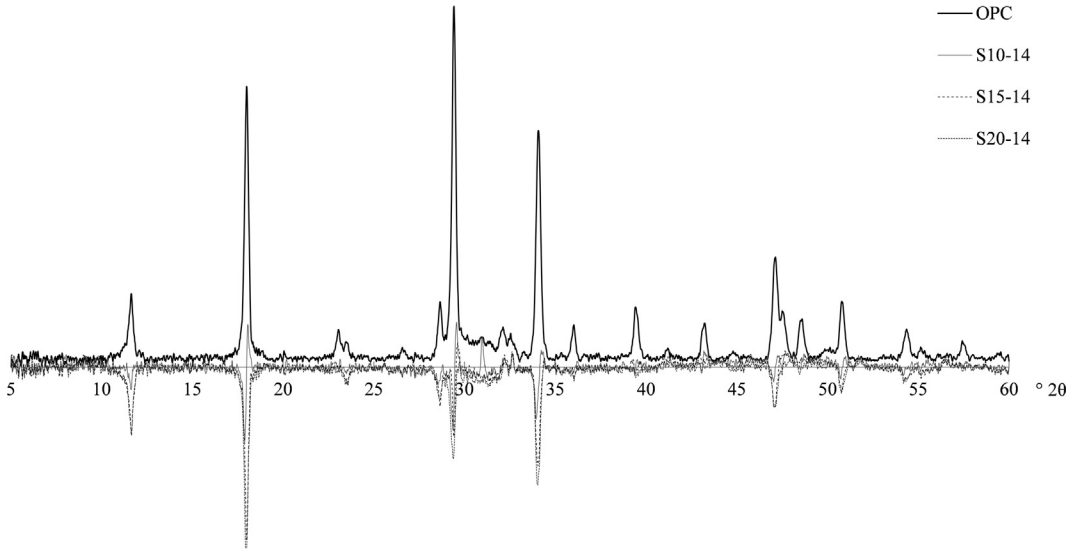

Fig. 7. Differential plot of XRD patterns of selected samples. Effect of silica concentration on peak intensity. More negative reflections indicate a lower content of the identified phase.

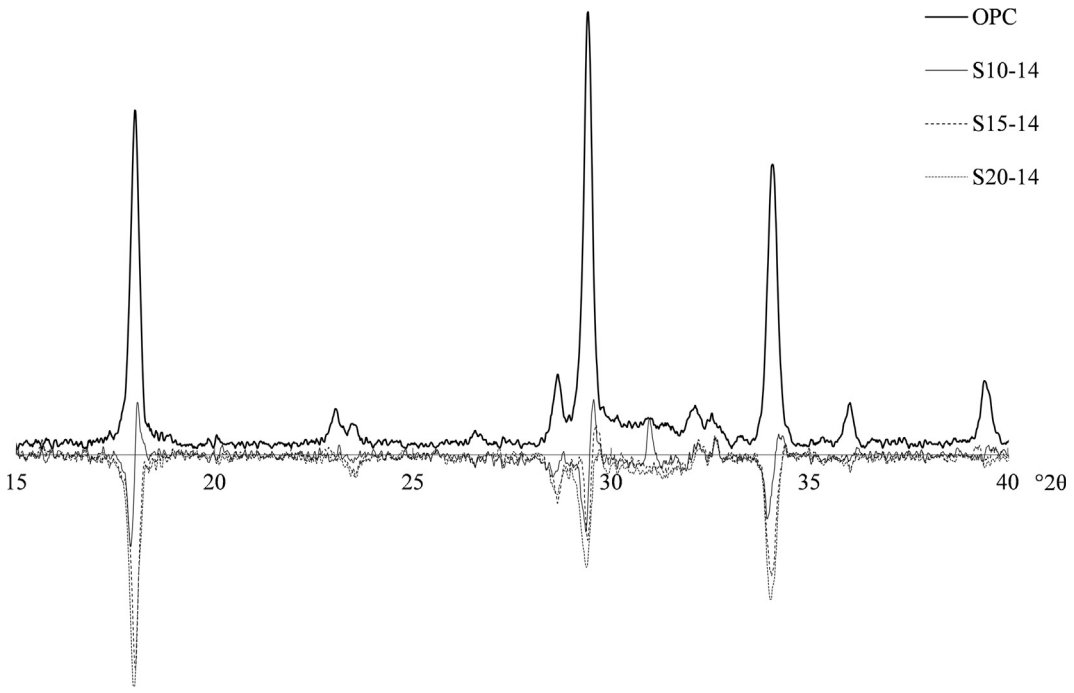

Fig. 8. Detail-zoom of Fig. 7. Differential plot of XRD patterns of selected samples. Effect of silica concentration on peak intensity. More negative reflections indicate a lower content of the identified phase.

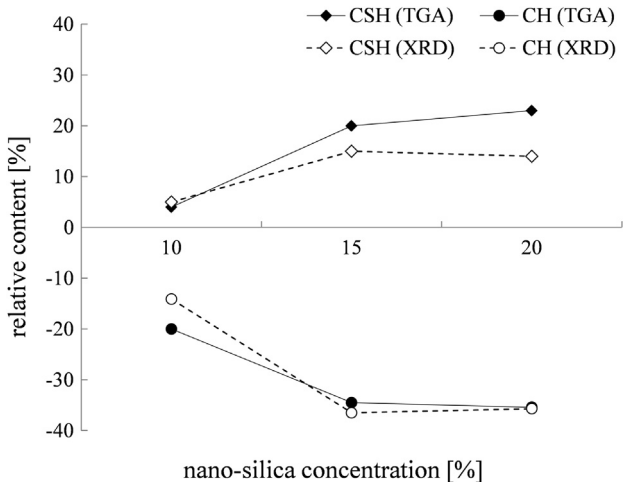

Fig. 9. Effect of nano-silica solution wt.% on relative increase of C-S-H and decrease of CH compared to the OPC control sample for 14 days of injection. Comparison between TGA results and semiquantitative results based on XRD data.

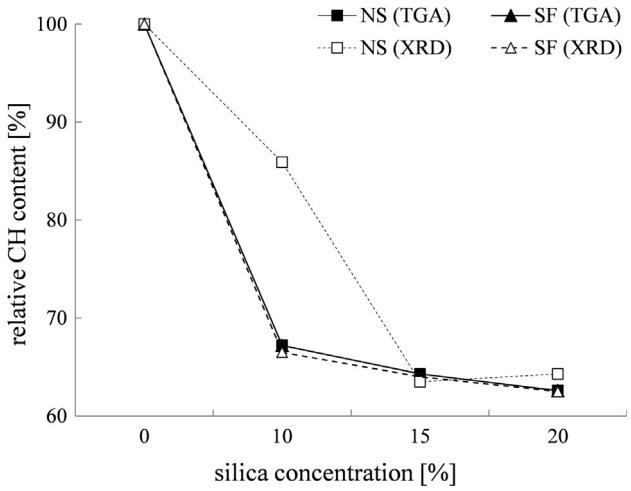

Fig. 10. Effect of silica particle-size and concentration on the CH relative content after 14 days of injection. Comparison between TGA results and semi-quantitative results based on XRD data.

result from silica and precipitated C-S-H creating pockets of isolated pores thus restricting the pore volume able to be experimentally observed. The reactivity of nano-silica with portlandite has been confirmed through SEM images, TGA and semi-quantitative XRD: particles move through the pores by diffusion, precipitate on portlandite crystals and react with calcium hydroxide forming additional C-S-H or C-A-S-H. Unreacted nano-silica was also observed, lying on the surface of cement paste or occluding pores and void space.

4. Conclusions

In this work we present a novel concrete and cement surface treatment. The following conclusions can be drawn:

1. Low-pressure (20 kPa) silica injection has effectively impregnated cement samples. After 14 days of injection with a nano-silica suspension of 20 wt.% concentration we observed a total reduction of 30% in porosity from the starting value, suggesting this is a potential consolidant for friable or cracked concrete.
2. Nano-silica injection is more efficient than silica fume, due to its smaller particle size allowing it to penetrate further into the pore structure and react to produce more C-S-H.
3. Some of the silica injected has reacted with the calcium hydroxide naturally present in hydrated cement, forming additional binding phases such as C-S-H and C-A-S-H. Unreacted silica however has been absorbed and acts as a filler agent reducing porosity.

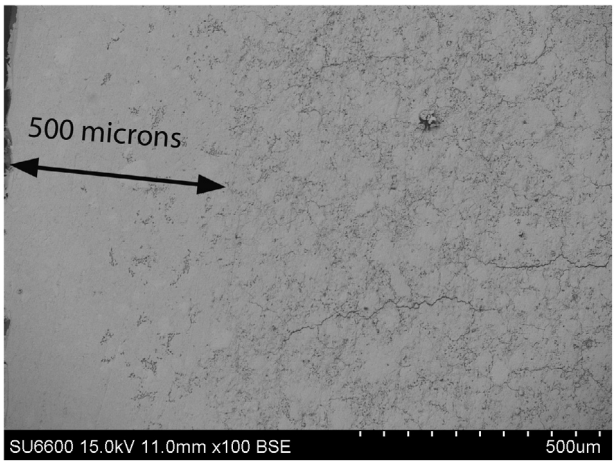

Fig. 11. BSE-SEM image of samples S10-14 and silica-front measurement.

4. After 14 days of nano-silica injection an average penetration depth of ca. 500 μm of was estimated from BSE-SEM images, which is ca. 20% of the cross section of the sample (4 mm).

Acknowledgements

This work is supported by EPSRC (Grant No. EP/L014041/1 - the DISTINCTIVE Consortium). Data associated with research published in this paper is accessible at http://dx.doi.org/10.15129/5e11a2f0-330a-4ed4-84a5-864b55f44371.

References

[1] A.J. Allen, J.J. Thomas, H.M. Jennings, Composition and density of nanoscale calcium-silicate-hydrate in cement, Nat. Mater. 6 (2007) 311–316, http://dx.doi.org/10.1038/nmat1871.

[2] J. Björnström, A. Martinelli, A. Matic, L. Börjesson, I. Panas, Accelerating effects of colloidal nano-silica for beneficial calciumsilicatehydrate formation in cement, Chem. Phys. Lett. 392 (2004) 242–248, http://dx.doi.org/10.1016/j.cplett.2004.05.071.

[3] H.E. Cardenas, L.J. Struble, Electrokinetic nanoparticle treatment of hardened cement paste for reduction of permeability, J. Mater. Civil Eng. 18 (2006) 554–560, http://dx.doi.org/10.1061/(ASCE)0899-1561(2006)18:4(554). http://ascelibrary.org/doi/abs/10.1061/(ASCE)0899-1561(2006)18:4(554).

[4] J.J. Chen, J.J. Thomas, H.F. Taylor, H.M. Jennings, Solubility and structure of calcium silicate hydrate, Cem. Concr. Res. 34 (2004) 1499–1519, http://dx.doi.org/10.1016/j.cemconres.2004.04.034. http://www.sciencedirect.com/science/article/pii/S000888460400211X.

[5] B.J. Christensen, T.O. Mason, H.M. Jennings, Comparison of measured and calculated permeabilities, Cem. Concr. Res. 26 (1996) 1325–1334.

[6] K. Garbev, M. Bornefeld, G. Beuchle, P. Stemmermann, Cell dimensions and composition of nanocrystalline calcium silicate hydrate solid solutions. Part 1: Synchotron-based X-Ray Diffraction, J. Am. Ceram. Soc. 91 (2008) 3015–3023, http://dx.doi.org/10.1111/j.1551-2916.2008.02601.x.

[7] C. Hall, W.D. Hoff, Water Transport in Brick, Stone, and Concrete, 2012. <https://www.crcpress.com/Water-Transport-in-Brick-Stone-and-Concrete/Hall-Hoff/p/book/9780415564670#googlePreviewContainer>.

[8] P. Hou, X. Cheng, J. Qian, S.P. Shah, Effects and mechanisms of surface treatment of hardened cement-based materials with colloidal nanoSiO_2 and its precursor, Constr. Build. Mater. 53 (2014) 66–73, http://dx.doi.org/10.1016/j.conbuildmat.2013.11.062. http://www.sciencedirect.com/science/article/pii/S0950061813010957.

[9] P. Hou, X. Cheng, J. Qian, R. Zhang, W. Cao, S.P. Shah, Characteristics of surface-treatment of nano-SiO_2 on the transport properties of hardened cement pastes with different water-to-cement ratios, Cem. Concr. Compos. 55 (2015) 26–33, http://dx.doi.org/10.1016/j.cemconcomp.2014.07.022. http://www.sciencedirect.com/science/article/pii/S0958946514001401.

[10] T. Ji, Preliminary study on the water permeability and microstructure of concrete incorporating nano-SiO_2, Cem. Concr. Res. 35 (2005) 1943–1947, http://dx.doi.org/10.1016/j.cemconres.2005.07.004. http://www.sciencedirect.com/science/article/pii/S0008884605001766.

[11] B.W. Jo, C.H. Kim, G.H. Tae, J.B. Park, Characteristics of cement mortar with nano-SiO_2 particles, Constr. Build. Mater. 21 (2007) 1351–1355, http://dx.doi.org/10.1016/j.conbuildmat.2005.12.020. http://www.sciencedirect.com/science/article/pii/S095006180600136X.

[12] D.S. Klimesch, A. Ray, J.P. Guerbois, Differential scanning calorimetry evaluation of autoclaved cement based building materials made with construction and demolition waste, Thermochim. Acta 389 (2002) 195–198, http://dx.doi.org/10.1016/S0040-6031(02)00058-8. http://www.sciencedirect.com/science/article/pii/S0040603102000588.

[13] H. Li, H.G. Xiao, J. Yuan, J. Ou, Microstructure of cement mortar with nano-particles, Compos. Part B: Eng. 35 (2004) 185–189, http://dx.doi.org/10.1016/S1359-8368(03)00052-0. http://www.sciencedirect.com/science/article/pii/S1359836803000520.

[14] R.M. Pellenq, N. Lequeux, H. van Damme, Engineering the bonding scheme in CSH: the iono-covalent framework, Cem. Concr. Res. 38 (2008) 159–174, http://dx.doi.org/10.1016/j.cemconres.2007.09.026. http://www.sciencedirect.com/science/article/pii/S0008884607002372.

[15] Y. Qing, Z. Zenan, K. Deyu, C. Rongshen, Influence of nano-SiO_2 addition on properties of hardened cement paste as compared with silica fume, Constr. Build. Mater. 21 (2007) 539–545, http://dx.doi.org/10.1016/j.conbuildmat.2005.09.001. http://www.sciencedirect.com/science/article/pii/S0950061805002837.

[16] F. Sanchez, K. Sobolev, Nanotechnology in concrete: a review, Constr. Build. Mater. 24 (2010) 2060–2071, http://dx.doi.org/10.1016/j.conbuildmat.2010.03.014. http://www.sciencedirect.com/science/article/pii/S0950061810001625.

[17] M. Sánchez, M. Alonso, R. González, Preliminary attempt of hardened mortar sealing by colloidal nanosilica migration, Constr. Build. Mater. 66 (2014) 306–312, http://dx.doi.org/10.1016/j.conbuildmat.2014.05.040. http://www.sciencedirect.com/science/article/pii/S0950061814005236.

[18] W. Sha, Advances in Building Technology, vol. I, Elsevier, 2002, http://dx.doi.org/10.1016/B978-008044100-9/50111-X. http://www.sciencedirect.com/science/article/pii/B978008044100950111X.

[19] W. Sha, E. O'Neill, Z. Guo, Differential scanning calorimetry study of ordinary Portland cement, Cem. Concr. Res. 29 (1999) 1487–1489, http://dx.doi.org/10.1016/S0008-8846(99)00128-3. http://www.sciencedirect.com/science/article/pii/S0008884699001283.

[20] S. Shaw, C. Henderson, B. Komanschek, Dehydration/recrystallization mechanisms, energetics, and kinetics of hydrated calcium silicate minerals: an in situ TGA/DSC and synchrotron radiation SAXS/WAXS study, Chem. Geol. 167 (2000) 141–159, http://dx.doi.org/10.1016/S0009-2541(99)00206-5. http://www.sciencedirect.com/science/article/pii/S0009254199002065.